

Physical, optical, thermoanalytical, and radiation response study of Eu_2O_3 -doped zinc fluoro-telluroborate glasses

A Wagh^{1*}, A N D'Souza², N Karunakara^{3,4}, H Shailaja¹, Y Raviprakash² and S D Kamath^{2*}

¹Department of Physics, Mahatma Gandhi Memorial College, Mangalore University, Udupi 576102, India

²Department of Physics, Manipal Institute of Technology, Manipal Academy of Higher Education, Manipal 576104, India

³Centre for Application of Radioisotopes and Radiation Technology (CARRT), Mangalore University, Mangalagangothri, Konaje, Mangalore, Karnataka, India

⁴Centre for Advanced Research in Environmental Radioactivity (CARER), Mangalore University, Mangalagangothri, Konaje, Mangalore, Karnataka, India

Received: 21 December 2021 / Accepted: 17 November 2022 / Published online: 4 January 2023

Abstract: In the present study, Eu^{3+} -doped zinc fluoro-telluroborate transparent glasses were prepared by the conventional melt–quench technique. Their density and refractive index values were measured, and using these values, different physical parameters (number density, oxygen packing density, no. of bonds/vol, etc.) were calculated and analysed. The XRD pattern displayed a disordered atomic arrangement in the glass network. The EDS spectra proved the purity of the samples exhibiting only those elements used during the synthesis. The good solubility of Eu^{3+} ions in zinc fluoro-telluroborate glasses was analysed through fine absorption peaks in the UV–Vis–NIR range. The absorption intensities increased in all samples up to 3.0 mol% of Eu^{3+} -doping concentration. The stabilities of the samples, such as $\Delta T \sim (144\text{--}156)^\circ\text{C}$ and $H_r \sim 2.33\text{--}4.00$, calculated using characteristic temperatures (T_g , T_x , T_c , T_m) from DSC studies exhibited their promising candidature in a high-temperature environment. The Eu7 (Eu^{3+} with 3.0 mol%) glass confirmed better attenuation properties (LAC, Z_{eff} , HVL, MFP) compared to other composition (0–2.5 mol%) glasses.

Keywords: Eu^{3+} ; NBO; T_g ; LAC; MFP

1. Introduction

Trivalent rare-earth (RE)-doped glasses have been researched for some years and realized their potential applications such as lasers, light-emitting diodes (LED), colour displays, sensors, optical fibre amplifiers, etc., in the optics and photonics field. The potential applications are attributed to the rare-earth elements' (REEs) superior absorption in UV–Vis–NIR spectral region, long lifetime, dominant emission, and high quantum efficiency. REEs can be doped into hosts like phosphors, nanowires, fuel cells, etc. Among them, glass hosts are very much preferred and stabilized for REEs. The RE doping is amenable when incorporated in large concentrations as they have high optical

homogeneity, large optical transparency window including UV–Vis–NIR range, and low nonlinear refractive index [1].

Developing optically active RE-doped glasses with appropriate composition of REEs and host matrix elements can be used in biomedical lasers, underwater and satellite communications, bar code reading, optical data storage, high-level waste storage from nuclear power plants, etc. Hence, the suitable combination of REE and host matrix and the right amount of each concentration will make the glass sample ready for different applications.

The REEs show sharp absorption/excitation and emission bands. The intense bands are accredited to the shielding effects of 4f electrons by $5s^2$ and $5p^6$ shells, i.e. screening 4f electrons from the crystal field perturbation. Due to this shielding effect, RE ions conserve their optical properties even though they get doped into different host matrices. RE ions depend less on the ligand field environment [1–3].

*Corresponding author, E-mail: akshathawagh@gmail.com; sudha.kamath@manipal.edu

Eu^{3+} ions are the most preferred among seventeen different REEs due to their simple energy-level structure. The Eu^{3+} ions have singlet ${}^7\text{F}_0$ ground state and ${}^5\text{D}_0$ excited states, which are non-degenerate under symmetry. It helps in estimating the local field environment of different host matrices.

Assessing a suitable host matrix for RE ions plays a crucial role in developing quality optoelectronic devices, as the glass optical properties and RE ion's quantum efficiencies depend entirely on the nature of the ligand environment around the RE ion site. Low phonon energy of the host matrix also results in good optical properties of the glass, else the incident energy is lost as heat loss within the lattice vibrations.

Several host matrices like silicate (SiO_2), phosphate (P_2O_5), tellurite (TeO_2), and germanate (GeO_2) are worked over. Among them, borate (B_2O_3) glasses exhibit salient features when doped with RE ions due to their high thermal stability, low melting point, and good RE ion solubility. The only drawback following the B_2O_3 glasses is its high phonon energy ($\sim 1300\text{--}1500\text{ cm}^{-1}$), which leads to non-radiative transitions that restrict the glass applications. To overcome such complications, low phonon energy halide (fluoride) compounds like ZnF_2 , PbF_2 , CaF_2 , and BaF_2 can be included in the glass matrix to improve the optical properties and the quantum efficiency [4, 5].

TeO_2 is a conditional glass former which practically cannot form glass single-handedly. It must be incorporated with another strong glass former to develop a strong, optically active glass. In the present study, TeO_2 is used in the matrix for the practical advantages of the sample, such as high refractive indices and high transparency in the IR region and majorly to reduce the phonon energy of the base host compound (B_2O_3).

Borate glasses have radiation-shielding properties due to their excellent thermal stability. To study the nuclear radiation shielding abilities of these glasses, different parameters like linear attenuation coefficient (LAC), effective atomic number (Z_{eff}), half value layer (HVL), and mean free path (MFP) were simulated with the help of PhyX/PSD simulation software in the photon energy range of 0.015–15 MeV [6–8].

With the advent of aerospace and nuclear (scientific and medical) technological applications, researchers all over the globe are looking into pursuing modern optical/electronic high-tech industrial advancements to overcome the influence of high ionizing radiations like heavy charged particles, electrons, protons, high energy photons, etc. Exposure to such charged particles leads to malfunctioning/failure in the operations of electronic circuits of spacecraft [9].

The primary goal is to protect the electronic components from the heavy charged particles/high energy photons of

the Earth's radiation belt, like fluxes of solar cosmic rays with energy up to $\sim 10^9$ eV and galactic cosmic rays with $\sim 10^{20}$ eV energies. The secondary particles produced due to the interaction of primary rays with shielding probes are more harmful than primary interactions [10]. According to Spratt et al. [11], the particle fluxes per 1mm^2 per year are ~ 30 particles with an energy of 10 GeV, $\sim 7 \times 10^{-3}$ particles with an energy of 1 TeV, and $\sim 1 \times 10^{-6}$ particles with an energy of 1 PeV. The galactic cosmic rays near the Earth's space are significantly different when collated with galactic cosmic rays in interstellar space due to the influence of the heliosphere (solar wind). Therefore, the sort of particles affecting the electronic components penetrating through the outer body of the spacecraft near the Earth's space and the outer space varies [12–15].

Protecting the discrete devices in the spacecraft/medical facilities from heavy charged particles/high energy photons through high-end radiation shielding materials is the pressing need of the hour. In this facet, simulating the interaction of such radiations with the materials used for shielding purposes is relevant. Thus, computer simulation (PhyX/PSD simulation software) of photons (here, gamma rays with different energies) transmission on the present experimental glasses is reported here.

In our present research article, the authors have assimilated borate, tellurite, and fluorides to form a zinc fluorotelluroborate glass network to set out non-hygroscopic, low phonon, and wide band gap samples, such that the samples can claim their potential candidatures in optoelectronic applications [16–18]. Aydin et al. [19] reported that fluoroborate glasses possess thermal stability in opposition to devitrification by doping rare-earth ions (here, Eu^{3+}). Zinc fluoroborate glasses are mainly used in high technological areas. Eu^{3+} doped in zinc fluoro-telluroborate glasses emits red light, which is a good approach for WLED applications through excitation from near UV or blue LED chips. As the world is focusing on green growth, sustainable life, and sound health, it is very much necessary that we look into such materials which contribute minimum towards global warming. As the demand for energy increases, the concern for climate change through greenhouse gases also escalates. So, WLEDs is an eco-friendly and energy-efficient light source which has proven its mettle through their high efficiency, small size, and long lifetime by replacing conventional fluorescent and incandescent lamps. WLEDs thus solve the rising issue of rapidly depleting reserves of fossil fuels and improving the quality of the global environment [20]. Suthanthirakumar et al. [21] have previously studied over similar matrix concentrating on the glasses' spectroscopic properties and claimed intense pure red emission from the same. In this article, the authors tried to bring out the samples' ability in high-temperature and high-energy

radiation environmental conditions. RE-doped optically active materials have promising time ahead as optical/electronic components and radiation shields [22]. Some other related works [1, 2, 23] on zinc fluoroborate glasses exhibit encouraging optical properties. The physical, optical, thermoanalytical, and radiation shielding parameter studies of such glasses would be constructive in material science and nuclear radiation fields.

2. Experimental details

A conventional melt–quench technique was employed in synthesizing Eu^{3+} -doped zinc fluoro-telluroborate glasses with matrix: 30 ZnF_2 – 20 TeO_2 – $(50 - x) \text{ B}_2\text{O}_3$ – $x \text{ Eu}_2\text{O}_3$ where $x = 0, 0.5, 1.0, 1.5, 2.0, 2.5, 3.0$ in mol%. The high-purity analytical grade (99.99%) chemical compounds procured through Sigma-Aldrich were weighed for their batches as tabulated in Table 1 and thoroughly mixed using an agate mortar pestle. The mixed compounds were then replaced in a porcelain crucible and kept for melting at 800 – 830 °C for 30 min in an electric furnace (type: Indfurr Superheat High-Temperature Furnace, Chennai, TN, India). After the melting period, the thus-formed molten mass was poured over a preheated (at 350 °C) stainless-steel mould. The annealing process (heat treatment) is done for 3 h on a hot plate (Indfurr Heating Furnace, Chennai, TN, India) to remove thermal or mechanical stress from glass samples.

Then, the samples are polished using different grit-size emery sheets and velvet polishing clothes on a grinding machine (type: Chennai Metco Bainpol, TN, India). To reduce friction during polishing, distilled water and diamond lubricant are used. The transparent break/crack free 2-mm-thick samples were ready after polishing for different characterizations. The samples were placed in a desiccator to avoid moisture absorption.

The glass samples were characterized for physical, structural, optical, thermal, and radiation shielding properties. The glasses' densities were measured through the Archimedes principle on a Contech Analytical weighing

machine Mumbai, India, with a precision of 0.1 mg. Xylene was used as an immersion liquid in the weighing machine. The refractive indices of the glasses were measured on Labman (LMAR-1317) Abbe digital refractometer with an accuracy of $\leq \pm 0.0002$. Clove oil was used as the reference and contact liquid during the experiment. The XRD of the samples was analysed under structural characterization. The XRD pattern was recorded operating on Rigaku Miniflex–600 X-ray Diffractometer with CuK_α radiation (40 kV and 15 mA) and a graphite monochromator with 2θ (θ being Bragg angle) within a range of 10° – 90° . The UV–Vis–NIR (250–2400 nm) absorption spectra of all the samples were recorded employing a PerkinElmer Lambda 750 s spectrometer. The energy-dispersive X-ray spectroscopy (EDS) spectra were recorded utilizing Zeiss EVO 18 system to investigate the successful incorporation and presence of the compounds used during the sample synthesis.

The DSC thermograms of the samples were recorded on NETZSCH STA 449 F3 Jupiter system. Glass powder (20 mg) of all the samples was examined in the temperature range of 30 – 1000 °C at a heat rate of 10 °C/min in nitrogen (N_2) gas atmosphere. The DSC data here are shown only within 300 – 900 °C (the range where useful data are obtained). The radiation shielding parameters were analysed using the PhyX/PSD simulation software.

The optical properties of the samples depend entirely upon Beer–Lambert's law (the thickness of all the samples was maintained at 2 mm). The law establishes a relation between the properties of the substance and the attenuation of incident light through the substance. The law gives a direct relation of absorbance of light with the molar absorption coefficient (ϵ), molar concentration (c), and optical path length (distance travelled by the light through the sample) (l).

$$A = \epsilon cl \quad (1)$$

According to the above law, when a monochromatic light ray passes through an absorbing material medium, the intensity of the light exponentially decreases as the length (l)/thickness of the samples increases. Hence, thinner and crack-free samples are the finest for optical studies. So, 2-mm-thick and finely polished samples are prepared for characterization. And maintaining 2-mm thickness for all the samples gives corresponding results, or else the results cannot be comparable in different thickness samples.

Table 1 Nominal chemical composition (mol%) of all synthesized glasses

Sample code	B_2O_3	TeO_2	ZnF_2	Eu_2O_3
Eu1	50	20	30	0
Eu2	49.5	20	30	0.5
Eu3	49.0	20	30	1.0
Eu4	48.5	20	30	1.5
Eu5	48.0	20	30	2.0
Eu6	47.5	20	30	2.5
Eu7	47.0	20	30	3.0

3. Results and discussion

3.1. Physical properties

Various physical parameters are given in Table 2 for Eu1–Eu7 glasses and have been calculated using their measured

Table 2 Physical parameters of the studied glasses

Property	Sample Code						
	Eu1	Eu2	Eu3	Eu4	Eu5	Eu6	Eu7
Molecular weight (M_w) (g/mol)	97.755	99.166	100.577	101.989	103.4	104.812	106.223
Sample thickness (mm)	2	2	2	2	2	2	2
Density (ρ) (g/cm ³)	3.068	3.179	3.284	3.356	3.421	3.576	3.599
Molar volume (V_m) (cm ³ /mol)	31.862	31.194	30.626	30.390	30.225	29.309	29.514
Crystalline volume (V_c) (cm ³ /mol)	26.188	26.284	26.381	26.477	26.573	26.669	26.766
Volume deviation (V_o)	5.674	4.91	4.245	3.913	3.652	2.64	2.748
$d_{B-B}(\times 10^{-8})$ (m)	3.753	3.715	3.680	3.658	3.640	3.591	3.588
Number density (N) ($\times 10^{20}$) (ions/cm ³)	–	0.965	1.966	2.972	3.985	5.137	6.122
Oxygen packing density (OPD) (mol/l)	59.630	60.908	62.038	62.520	62.861	64.824	64.374
Refractive index (n)	1.529	1.555	1.573	1.608	1.627	1.653	1.671
Molar refraction (R_m) (cm ³ /mol)	9.826	10.012	10.091	10.508	10.712	10.729	11.038
Polaron radius (r_p) ($\times 10^{-8}$) (m)	–	8.786	6.930	6.038	5.476	5.031	4.746
Internuclear distance (r_i) ($\times 10^{-7}$) (m)	–	2.18	1.719	1.498	1.358	1.248	1.177
Field strength (F) ($\times 10^{15}$) (m ⁻²)	–	8.161	13.118	17.280	21.009	24.890	27.969
No. of bonds/vol. (n_b) ($\times 10^{28}$) (m ⁻³)	7.561	7.742	7.905	7.987	8.050	8.322	8.285
Electronic polarizability (α_{o^2-}) (n)	1.711	2.018	2.033	2.118	2.158	2.160	2.222
Molar electronic polarizability (α_m) ($\times 10^{-24}$) (cm ⁻³)	3.894	3.967	3.999	4.164	4.245	4.251	4.374
Metallization criterion (M)	0.691	0.679	0.670	0.654	0.645	0.633	0.626
Optical basicity (Λ)	0.693	0.842	0.848	0.881	0.896	0.896	0.918

density (ρ) and refractive indices (n) values. The densities of the glass samples were measured through the Archimedes principle. Density explains the structural softness or compactness. The immersion liquid used for the experiment is xylene ($\rho = 0.865$ g/cm³). The Contech Analytical Balance is programmed to display density values directly using the relation:

$$\rho = \frac{w_a}{w_a - w_b} \cdot \rho_b \quad (2)$$

where w_a is the weight in the air, w_b is the weight of xylene and ρ_b is the density of xylene.

The densities of the samples increased with an increase in Eu₂O₃ concentration in the glass matrices. The elevation in the values of densities is due to the substitution of lower molar mass B₂O₃ (M_w : 69.63 g/mol) with higher molar mass Eu₂O₃ (M_w : 351.926 g/mol) atoms. With the increase in the density values of the glasses, more molecules are present per volume, and more light is obstructed. Hence, the refractive indices (n) show a similar trend as densities.

Molar volume (V_m) indicates a spatial distribution of oxygen (O) atoms in the glass network. The molar volume of the samples decreased with an increase in Eu₂O₃ content and an increase in the density values. This subsequent change in ' V_m ' is a normal behaviour expected in glass systems. The steady reduction in the ' V_m ' values is

attributed to the dense nature of the glass network. The number of bonds per unit volume (n_b) values in Table 2 shows that n_b increases with an increase in Eu₂O₃ [24]. The n_b can be calculated by

$$n_b = \frac{N_A}{V_m} \sum_i (n_c x_i) \quad (3)$$

here ' n_c ' and ' x_i ' are the coordination number and concentration of the cations [25]. The increase in the n_b values attributes to the decrease in molar volumes of the present glasses (from Eu1 to Eu6). For Eu7 glass, a slight rise in molar volume is observed, and a small decrease in n_b value (Table 2). Here, Eu₂O₃ atoms after 2.5 mol% in the matrix stop playing the role of the modifier. In the amorphous network, at 3.0 mol% of Eu₂O₃ content, the dopant loses its capability of depolymerization, hence increasing the ' V_m ' and NBOs [26].

The studies have revealed that, with the increase in rare-earth content in the amorphous network, the spacing between the same decreases, which increases the magnitude of quenching in the properties due to ion clustering [3, 27–30]. Quenching occurs due to energy transfer between rare-earth ions in various network sites as the ion concentration increases.

The volume occupied by 1 mol of a substance (V_m) decreases. This recommends modifying the B-to-O ratio,

which converts tetrahedral BO_4 units to trigonal BO_3 units. This results in the formation of a number of non-bridging oxygens (NBOs) [25, 31, 32].

The Eu^{3+} plays the role of dopant ion. They act as network modifiers that weaken the BO_4 tetrahedral units' network by breaking B–O bonds, thus creating structural defects like NBOs producing tricluster/trigonal O bonds with B network former. The $(\text{BO}_3/\text{BO}_4)$ ratio in the glass network controls the physical properties of glasses. Subsequently, the $(\text{BO}_3/\text{BO}_4)$ ratio depends upon the annealing temperature and/or dopant concentration in the amorphous network. The Eu^{3+} opens the amorphous structural network breaking the BO_4 symmetry and producing NBOs that make the network open and ready to accept more modifiers. NBOs are O dangling bonds or permanently broken O bonds, which are localized defects in the glass networks.

All the physical parameters directly depend upon the presence of such defects. Physical laws ascertain that polarizability is directly proportional to the refractive index and the NBOs present in the network [1, 4, 32, 33]. NBO ions possess higher polarizability in contrast to bridging oxygens (BOs). So, the refractive index values were found to increase with assumed NBOs.

The molar refraction (R_m) values are acquired following the formula given below,

$$R_m = \left(\frac{n^2 + 1}{n^2 + 2} \right) \left(\frac{M_w}{\rho} \right) \quad (4)$$

' R_m ' specifies the average refraction of isotropic substances like glasses. When Avogadro's number (N_A) is introduced in ' R_m ,' it can be expressed as a function of molar electronic polarizability (α_m) which is obtained using the relation:

$$\alpha_m = \left(\frac{3}{4\pi N_A} \right) \cdot R_m \quad (5)$$

The ' R_m ' indicates the cationic refraction and O ion reaction. An increase in ' R_m ' with an increase in refractive indices values and oxygen packing density (OPD) specifies the bonding of the ions in the glasses. The OPD is the number of O atoms per molecular weight of the samples, and it is calculated using the relation,

$$\text{OPD} = \left(\frac{\rho}{M_w} \right) \cdot n \cdot 1000 \quad (6)$$

where n is the number of O atoms in each oxide [25, 32].

Electronic polarizability ($\alpha_{o^{2-}}(n)$) of ions expresses the deformation of the electronic clouds on applying electromagnetic fields. It is closely related to properties like molar refraction (R_m) and optical basicity (Λ). Relatively, electronic polarizability ($\alpha_{o^{2-}}(n)$) and molar electronic polarizability (α_m) values were observed to increase with the

increase in refractive indices of the glass samples. The decrease in V_m proves the decrease in polaron radius (r_p) and internuclear distance (r_i) with the increase in Eu^{3+} content and number density (N) in the glasses. The N suggests the number of Eu^{3+} ions/unit volume in the glass network.

The electronic polarizability ($\alpha_{o^{2-}}(n)$), polaron radius (r_p), and internuclear distance (r_i) can be calculated following the relation [34] given below,

$$\alpha_{o^{2-}}(n) = \left[\left(\frac{R_m}{2.52} \right) - \sum \alpha_i \right] (N_{o^{2-}})^{-1} \quad (7)$$

$$r_p = \left(\frac{1}{2} \right) \left(\frac{\pi}{6N} \right)^{1/3} \quad (8)$$

$$r_i = \left(\frac{1}{N} \right)^{1/3} \quad (9)$$

The ' r_p ' describes interactions between electrons and ions. The ' r_p ' is theoretically expected to be less than the interionic distance (r_i), i.e., the distance between two nearby ions and the results obtained manifest the same.

This indicates that the atoms are densely packed in the Eu^{3+} -doped zinc fluoro-telluroborate glasses, and so is the field strength (F) [$F = \left(\frac{Z}{r_p} \right)$] results.

According to Fajan's rule, given in Dimitrov et al. [35], the polarizability of cation increases in the Coulomb field of the anion with an increase in its positive charge. As per the theory, in the condensed state of a matter, the charge distribution of each negative or positive ion can be distorted by the nearby another ion. That is, the polarizability or the loosening or tightening of the electron clouds entirely depends upon chemical binding forces. Hence, the ($\alpha_{o^{2-}}(n)$), (α_m), and (R_m) was perceived to be increasing with an increase in Eu^{3+} cations in the glass network.

As per the study done by Duffy and Ingram given in Dimitrov et al. [36], the optical basicity (Λ) is the measure of acid–base properties of glasses, alloys, molten salts, etc. It is a numerical expression that gives the electron donor power of oxide species in the medium. As per the results obtained following the expression,

$$\Lambda = 1.67 \left(1 - \frac{1}{\alpha_{o^{2-}}} \right) \quad (10)$$

the values increased with an increase in Eu^{3+} concentration, which advised the increasing ability of electron exchange between ions in the glass network. It is said that if ($\alpha_{o^{2-}}(n)$) and Λ possess small values [$((\alpha_{o^{2-}}(n)) = 1.4–1.6)$, ($\Lambda = 0.4–0.6$)], then the glasses are acidic. But in the current case, the ($\alpha_{o^{2-}}(n)$) values are high, and range between (1.711–2.222) and values of Λ is

between (0.693–0.918), which proves the basicity (basic nature) of the present experimented glass samples [35–39].

With the increase in polarization, the valence electrons in their quasi-elastic state in their respective atoms are set free through neutral polarization in their condensed state, becoming free electrons promoting the amorphous material towards metallic nature. To prove the metallic criterion of any given sample in its condensed state, $\frac{R_m}{V_m} > 1$ is considered a metal and $\frac{R_m}{V_m} < 1$ is taken as an insulator.

This parameter is named as metallization criterion (M) obtained as $M = 1 - \frac{R_m}{V_m}$.

Following this, non-metallic/metallic behaviour of the glasses can be analysed. Samples with a large value of ' M ' (close to 1) are considered insulators, and with a small ' M ' (close to 0), the samples are metallic. In samples with a small ' M ', the conduction and valence band width largely results in a narrow band gap and an increase in the metallicity of the glass samples [40].

A related trend in the results of crystalline volume (V_c) of the glasses is seen in Table 2. The ' V_c ' of the glasses gradually increased with an increase in Eu^{3+} content. The ' V_c ' values are obtained following the expression, $V_c = \sum x_i V_i$, where ' V_i ' is the crystalline volume of the compound. With the tendency of the glasses towards metallic nature, the ' V_c ' is observed to increase. Volume deviation (V_o) obtained by $(V_m - V_c)$ indicates the reducing amorphous network in the glasses with an increase in Eu^{3+} content.

The average Boron–Boron separation ($\langle d_{B-B} \rangle$) is calculated using,

$$\langle d_{B-B} \rangle = \left(\frac{V_m^B}{N_A} \right)^{1/3} \quad (11)$$

where ' V_m^B ' is the molar volume of B atoms in the network, i.e. a volume that contains 1 mol of B atoms within the amorphous network. The molar volume of B is taken as $V_m^B = \frac{V_m}{2(1-x_B)}$. Here, ' x_B ' is the molar fraction of B_2O_3 oxide. The $\langle d_{B-B} \rangle$ gives insights into the modification of the glass network due to the Eu^{3+} ion doping. Boron atoms are central atoms with negatively charged tetrahedral units (BO_4^-). The decrease in $\langle d_{B-B} \rangle$ values with an increase in Eu^{3+} concentration in the glasses relates to the presumption of conversion of BO_4 to BO_3 units forming NBOs in the network [41].

3.2. X-ray diffraction (XRD) analysis

The overlaid broad hump in Fig. 1 around $2\theta = 22^\circ$ – 37° is the diffracted X-ray peaks from the amorphous network of the Eu^{3+} -doped glasses. The broad diffracted peaks

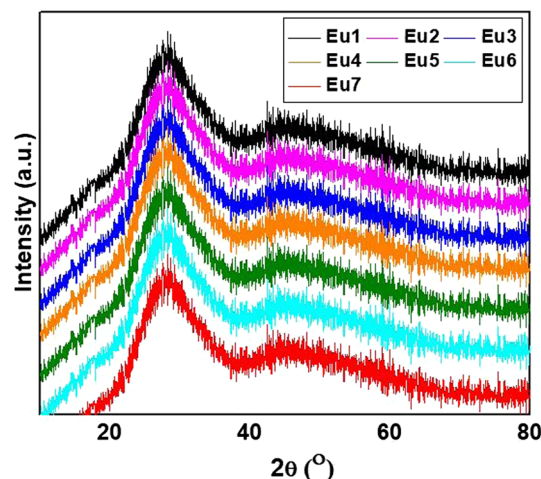


Fig. 1 Overlaid XRD patterns of the ZnF_2 – TeO_2 – B_2O_3 – Eu_2O_3 glass samples

indicate the disordered long-range atomic arrangements in the amorphous structure of the samples [42].

3.3. Energy-dispersive X-ray spectroscopy (EDS) analysis

The EDS spectra of Eu1, Eu3, Eu5, and Eu7 samples in Fig. 2 revealed the presence of all the elements (Zn, F, Te, O, B, Eu) used for the synthesis of the same. The use of crucibles and stainless-steel mould for preparing the samples did not significantly change the samples' purity [43].

3.4. UV–Vis–NIR absorption analysis

Figure 3 (a) and (b) shows the overlaid UV–Vis–NIR absorption spectra of Eu^{3+} -doped zinc fluoro-telluroborate glasses, recorded within the wavelength range (350–2400) nm. The UV–Vis spectra show six absorption bands at around 380 nm (${}^7\text{F}_0 \rightarrow {}^5\text{L}_6$), 445 nm (${}^7\text{F}_0 \rightarrow {}^5\text{D}_2$), 510 nm (${}^7\text{F}_0 \rightarrow {}^5\text{D}_1$), 520 nm (${}^7\text{F}_1 \rightarrow {}^5\text{D}_1$), 552 nm (${}^7\text{F}_0 \rightarrow {}^5\text{D}_0$), and 560 nm (${}^7\text{F}_1 \rightarrow {}^5\text{D}_0$) and two absorption bands at around 2100 nm (${}^7\text{F}_0 \rightarrow {}^7\text{F}_6$) and 2200 nm (${}^7\text{F}_1 \rightarrow {}^7\text{F}_6$).

The Eu^{3+} ions get excited from ${}^7\text{F}_0$ and ${}^7\text{F}_1$ states to various higher energy states. The ${}^7\text{F}_0$ and ${}^7\text{F}_1$ states have a small energy gap between ($\sim 350 \text{ cm}^{-1}$) them, which results in fractional ion excitation from ${}^7\text{F}_1$ states as well. Forty-five percentage of electrons are studied to be populated at ${}^7\text{F}_0$ energy state, and 35% of electrons are populated at ${}^7\text{F}_1$ energy state. The ${}^7\text{F}_0 \rightarrow {}^5\text{D}_2$ absorption transition at around 445 nm is observed to have the highest intensity compared to other transitions of Eu^{3+} ions. The ${}^7\text{F}_0 \rightarrow {}^5\text{D}_2$ transition is evaluated as a hypersensitive electric dipole transition due to the $\Delta L, \Delta J \leq 2$ selection rules. The intensity of this transition depends upon the surrounding medium. The magnetic dipole transition, ${}^7\text{F}_0$

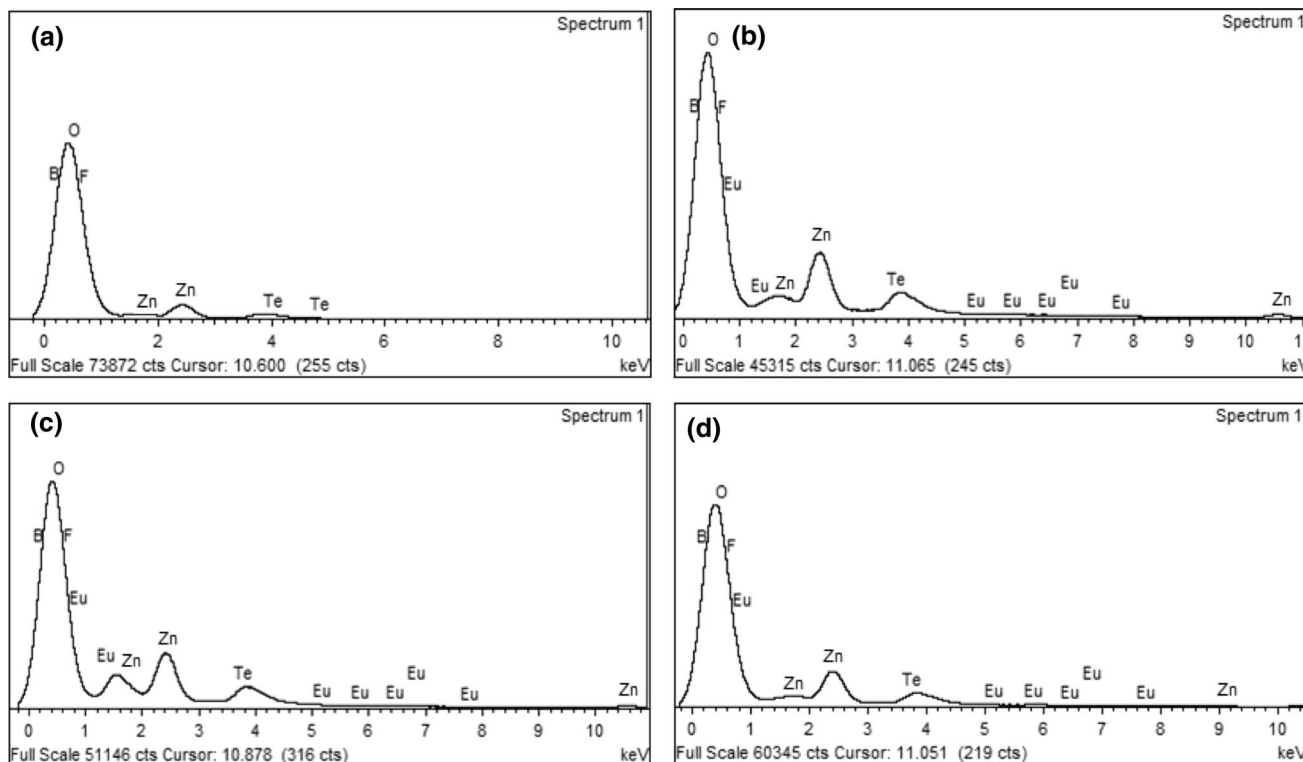


Fig. 2 EDS spectra of (a) Eu1, (b) Eu3, (c) Eu5 and (d) Eu7 glasses

$\rightarrow {}^5D_1$, is observed to have less intensity than the electric dipole transition, and it does not condition on ligand field environment [44].

Due to the spectrometer's poor intensity, the 5D_4 and 5D_3 transitions are not observed in absorption spectra. The ${}^7F_0 \rightarrow {}^5L_6$ transition follows $|\Delta S| = 0, |\Delta L| \leq 2$ and $|\Delta J| \leq 2$ selection rule. This transition is also known as a hypersensitive transition, which entirely depends upon the host matrix and ligand environment of the Eu^{3+} ions. The NIR region has two intra-configurational f-f transitions, ${}^7F_0 \rightarrow {}^7F_6$ and ${}^7F_1 \rightarrow {}^7F_6$. With the increase in Eu^{3+} content, the cut-off energy values showed red-shift (longer wavelength side) extending to the blue region of the electromagnetic spectrum. The strong absorption of ${}^7F_0 \rightarrow {}^5D_2$ transitions in the blue region around 445 nm possesses great application for phosphor-converted W-LEDs (for generating WLEDs near UV or blue LED chip is required). The intensities of the absorption peaks continuously increased to 3.0 mol% of Eu^{3+} ions in the samples, except for the ${}^7F_0 \rightarrow {}^5L_6$ band [1, 4, 45].

3.5. Band gap (E_g) and Urbach energy (ΔE) analysis

The optical band is an effective probe for studying the electronic band structure of atoms. Incident energy gets absorbed by any optical material only when the photon energy is greater than the optical band structure of the

material. Generally, the band gap is the difference between the top of the valence band and the bottom of the conduction band.

The optically induced transitions are obtained from the absorption coefficient ($\alpha(\vartheta)$) near the fundamental absorption edge. The $\alpha(\vartheta)$ can be calculated following the equation below,

$$\alpha(\vartheta) = \left(\frac{1}{d}\right) \ln\left(\frac{I_o}{I_t}\right) \quad (12)$$

where 'd' is the sample thickness, I_o and I_t are the incident and transmitted radiation intensities, respectively. Davis and Mott gave a relation relating $\alpha(\vartheta)$ and optical band gap (E_g),

$$\alpha(h\nu) = B(h\nu - E_g)^m \quad (13)$$

where 'B' is the band tailing parameter, E_g is the optical band gap energy, 'm' is an index that depends upon the indirect ($= 2$) and direct ($= \frac{1}{2}$) allowed transitions, respectively.

A graph of absorption coefficient with respect to photon energy $\alpha(h\nu)$ against photon energy ($h\nu$) exhibits Tauc's plot. When a straight line is extrapolated along the linear region of the Tauc's curve at $(\alpha h\nu)^2 = 0$ (for direct) and $(\alpha h\nu)^{\frac{1}{2}} = 0$ (for indirect), optical band gap of the samples can be obtained. Since borate glasses are associated with a

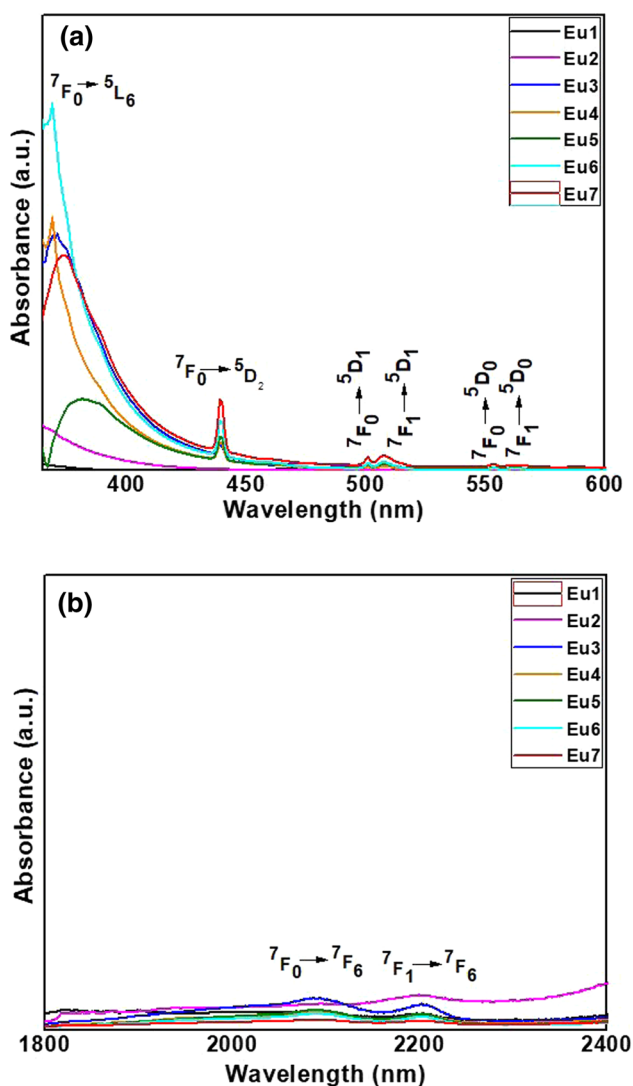


Fig. 3 Overlaid (a) UV–VIS and (b) NIR absorption spectra of the $\text{ZnF}_2\text{-TeO}_2\text{-B}_2\text{O}_3\text{-Eu}_2\text{O}_3$ glass samples

small amount of phonon energy, the samples are studied for only indirect allowed transition.

The optical band values for indirect ($m = 2$) allowed transitions in Eu^{3+} -doped zinc fluoro-telluroborate glasses are in the range of (2.87–2.67) eV. The ' E_g ' values for Eu1 to Eu7 samples are (0, 2.87, 2.76, 2.69, 2.68, 2.68, and 2.67) eV, respectively. The trend shows a decrease in band gap values with an increase in Eu^{3+} ion concentration. The decrease in ' E_g ' is validated with an increase in NBOs in the glass network causing structural changes [2, 46, 47]. The red shift in band edges and the decrease in energy required for an ion/electron to transit from the valence to the conduction band proclaimed alteration in the inter-linkage of oxygen bonding with the cations in the network [48, 49]. These out-turn in the production of NBOs.

The band tail width of the localized states is the Urbach energy (ΔE). The ' ΔE ' is extracted from the $\ln \alpha$ v/s photon

energy ($h\nu$) plot. The inverse slope of the plots gives the ' ΔE '. The empirical relation proposed by Urbach is,

$$\alpha(\nu) = \alpha_o \exp\left(\frac{h\nu}{\Delta E}\right) \quad (14)$$

' α_o ' is a constant, 'h' is Planck's constant, frequency is given as ' ν ', and Urbach energy is denoted as ' ΔE '. The ' ΔE ' values for Eu1 to Eu7 samples are 0, 0.165, 0.172, 0.186, 0.191, 0.201, and 0.282, respectively. The ' ΔE ' and ' E_g ' manifested opposite trends in the results. Low ' ΔE ' values suggested minimum defects (intrinsic atomic size defects (NBOs, dangling bonds) due to local deviation in the short-range arrangements) in the experimented glasses.

3.6. DSC analysis

Figure 4 exhibits overlaid DSC curves for Eu^{3+} -doped zinc fluoro-telluroborate glasses. Four different characteristic temperatures were extracted from the DSC thermograms, namely glass transition temperature (T_g), the onset of crystallization temperature (T_x), crystallization temperature (T_c), and melting temperature (T_m). These characteristic thermal parameters give a qualitative estimation of the samples' thermal stability and glass-forming ability [50, 51].

The ' T_g ' depends upon the structural units building the glass network and the kind of connectivity between the ions. The broad endothermic hump around 360–450 °C corresponds to ' T_g ', which initiates glass softening. The ' T_g ' represents the density cross-links between the ions and the rigidity of the glass-forming oxides. These characteristic temperatures reveal information about glass-forming ability and glass thermal stability. The characteristic temperatures with calculated stability factors are tabulated in Table 3 [50, 51].

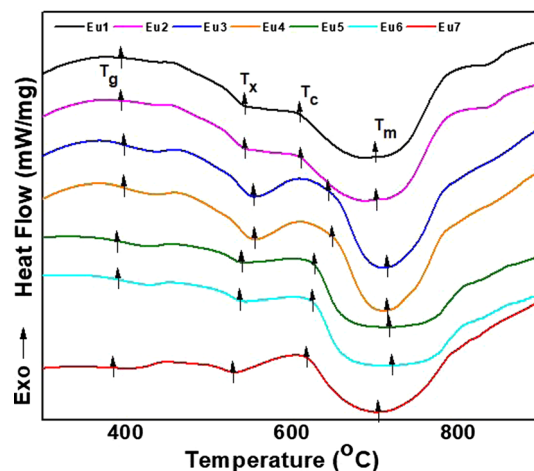


Fig. 4 Overlaid DSC thermograms of the $\text{ZnF}_2\text{-TeO}_2\text{-B}_2\text{O}_3\text{-Eu}_2\text{O}_3$ glass samples

Table 3 Characteristic temperatures (T_g , T_x , T_c , T_m) and the stability factors (ΔT , H_r) of the studied glasses

Sample code	T_g	T_x	T_c	T_m	ΔT	H_r
Eu1	393	542	608	700	149	2.336
Eu2	394	542	612	702	148	2.422
Eu3	397	553	642	716	156	3.310
Eu4	398	554	650	713	156	4.000
Eu5	389	538	626	718	149	2.571
Eu6	389	539	624	721	150	2.422
Eu7	385	529	619	704	144	2.752

An exothermic peak within the range of 570–640 °C represents crystallization temperature ' T_c ', and the onset of crystallization in the samples is marked as ' T_x '. The glasses showed only one broad peak representing crystallization at a heating rate of 10 °C/min. This proves that samples do not show any tendency towards nucleation and crystallization. At higher temperatures, another endothermic peak due to the remelting of glass is marked as ' T_m ' [50, 51].

The ' T_g ' of the samples revealed an increasing trend from 0 to 1.5 mol% and then a decreasing trend for 2.0 mol%, 2.5 mol%, and 3.0 mol% of Eu^{3+} content in the samples. The increase of ' T_g ' values validates the increase in ' n_b ' and ' ρ ' values. With the increase in ' n_b ', the ' T_g ' increased, but at a certain concentration of Eu_2O_3 in zinc fluoro-telluroborate matrix ' T_g ' showed a decreasing trend. This observation holds good because of the Boron anomaly taking place in the samples. With an increase in the modifier (Eu^{3+}) content in the borate network, there is an increase in trigonal boron atoms (BO_3) which incidentally tends toward the formation of NBOs. This verifies the results observed in physical parameters regarding the formation of NBOs. The increase and decrease in ' T_g ' corroborate the increased NBOs in the glass network (bonds per unit volume). The Boron anomaly happens due to the increased number of weak Eu–O linkages (473 kJ/mol) when compared to strong B–O linkages (806 kJ/mol). With the rise in weaker Eu–O linkages, there is a reduction in the density of cross-linkages in the glass network and thus resulting in a decrease of ' T_g ' at a higher Eu^{3+} content [50, 51].

Glass stability against devitrification is studied through the Dietzel factor ($\Delta T = T_x - T_g$) and Hruby's parameter ($H_r = \frac{T_c - T_g}{T_m - T_c}$). Glasses with high stability factor ($\Delta T < 100$ °C) and low-temperature interval ($T_m - T_c$) manifest the best candidature for fibre fabrication. The Eu^{3+} -doped zinc fluoro-telluroborate glasses showed relatively high stability values for $\Delta T \sim (144 - 156)$ °C and $H_r \sim 2.33 - 4.00$ (standard value of $H_r \sim 0.5$) representing

high thermal stability in the case of devitrification. These stability values thus promote the present set of glasses for different high-temperature applications, such as in a radiation environment [50, 51].

3.7. Radiation shielding properties

The linear attenuation coefficient (LAC) values were determined for the concerned glasses in the photon energy range of 0.015–15 MeV with the help of PhyX/PSD simulation software [52]. The graph in Fig. 5 interpreted the dramatic fall of LAC values for the initial photon energy range. Such fall can be justified by the photoelectric absorption of photons by glass material because this process is more likely to occur at lower energies. Further, at higher energies, LAC decreased at a slower rate. The rate of decrease in LAC values is different in low- and high-energy regions. For example, in Eu7 glass, we see that LAC decreases from 0.5058 to 0.2721 cm^{-1} for low-energy values between 0.283 and 0.662 MeV ($\Delta \text{LAC} = 0.2337 \text{ cm}^{-1}$), whereas $\Delta \text{LAC} = 0.2406 - 0.13827 \text{ cm}^{-1} = 0.10233 \text{ cm}^{-1}$ for high-energy values between 0.826 and 2.506 MeV. From this interpretation, the authors have concluded that shielding capacity is independent of energy for radiation of higher energy because of the predominance of the Compton scattering process. Further interaction of radiation photons by the pair production process leads to a slight rise in LAC values for energies above 10 MeV.

Similar results were reported for many other glass systems in the literature, and the LAC values at different energies were in good agreement with the values reported for Eu^{3+} -doped glasses by various researchers [6–8, 36, 53–55]. A discontinuity around 0.035 MeV corresponds to the K -absorption edge of the tellurium element. It was also observed (in Fig. 5) that at each energy, LAC increased with the increase in Eu_2O_3 concentration,

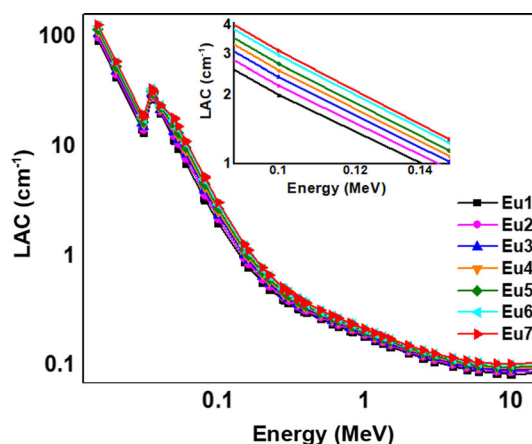


Fig. 5 LAC values varying with photon energy in the range of 0.015–15 MeV for Eu^{3+} -doped telluroborate glasses

which is more clearly seen in the inset of Fig. 5. Therefore, Eu7 glass acts as a glass shield with the highest attenuation property. This can be explained based on the increase in density with the increasing Eu_2O_3 mol% due to the replacement of lighter B_2O_3 molecules by heavier Eu_2O_3 molecules, as shown in Table 2.

A material having high Z_{eff} values contains more atoms to encounter the radiation photons, thus improving the radiation shielding property of that material. The following relation was utilized by PSD/Phy – X software [52, 56] to produce the Z_{eff} values in the 0.015–15 MeV photon energy region:

$$Z_{\text{eff}} = \frac{\sum f_i (\mu_m)_i}{\sum f_j \frac{A_j}{Z_j} (\mu_m)_j} \quad (15)$$

The graphical representation of the Z_{eff} values of Eu^{3+} -doped glasses is given in Fig. 6. There were no behavioural changes in Z_{eff} values between different doped glasses. Initially, at low gamma energies, the Z_{eff} of all the glasses decreases till 1 MeV, following which the values were constant in the 1–6 MeV region. Later for higher gamma energies, the values were found to increase with energy.

The discontinuities occurring in the low-energy region at 0.035–0.049 MeV are due to the K -absorption edges of Te and Eu elements, respectively. Photoelectric interaction is the main cause for the initial decreasing tendency because the cross-section of the photoelectric process depends on photon energy as $E^{-3.5}$. The predominance of Compton scattering in the intermediate energy region gives rise to constant Z_{eff} values in this region. Finally, due to the creation of electron–positron pairs caused by the interaction of glass particles with high-energy photons, the Z_{eff} values slightly rise [57].

The glass containing a higher concentration of Eu_2O_3 gave rise to high Z_{eff} values at all the energies above

0.03 MeV (Fig. 6). Therefore, the Eu7 glass sample with maximum Z_{eff} in the range of 17–37 is a better candidate for shielding gamma rays compared to other Eu^{3+} -doped glasses synthesized in the present work.

The fabricated Eu^{3+} -doped glasses were thoroughly investigated to determine other radiation shielding terms such as half value layer (HVL) and mean free path (MFP). The Phy – X/PSD software applied the following relations for calculating these two parameters,

$$\text{HVL} = \frac{0.693}{\mu} \quad (16)$$

$$\text{MFP} = \frac{1}{\mu} \quad (17)$$

The influence of photon energy on HVL values was established with the help of graphs shown in Fig. 7. Materials with low HVL and MFP values are most favoured for radiation shielding applications because of low material requirements when used as an attenuator against harmful radiation. In Fig. 7, HVL exhibited a flat line pattern at low gamma energy till 0.1 MeV with hardly any variation with sample composition. After 0.1 MeV, the values shot up continuously with the increasing photon energy. For Eu7 glass, HVL increased from 2.547 cm at 0.662 MeV to 3.485 cm at 1.173 MeV and 3.729 cm at 1.33 MeV. This indicates a greater thickness requirement for attenuating high-energy photons. Also, in terms of Eu_2O_3 content, HVL decreases from 8.214 cm to 7.237 cm to 6.529 cm at 15 MeV for Eu1, Eu4, and Eu7, respectively. The values of HVL calculated for the present glass systems are similar to those reported for other Eu-doped glasses in the literature [6, 7, 53]. Hence, the lowest set of HVL values observed for Eu7 glass confirmed better attenuation properties than other compositions.

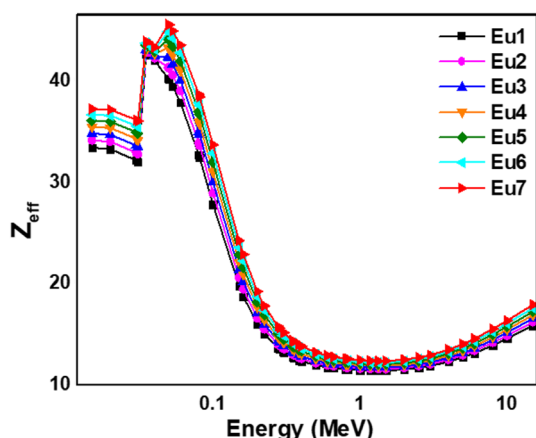


Fig. 6 Z_{eff} values varying with photon energy ranging from 0.015–15 MeV for the prepared Eu^{3+} -doped glass systems

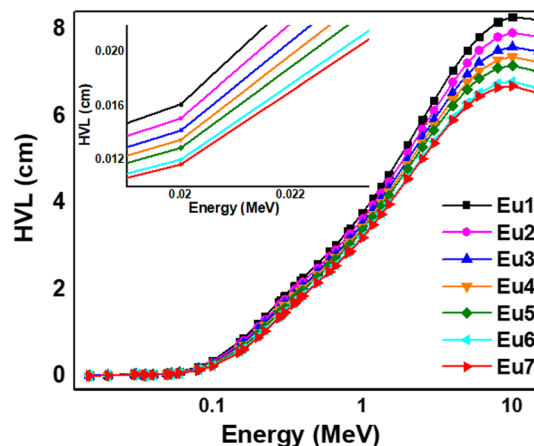


Fig. 7 Plot of HVL values for Eu3 +-doped telluro-borate glass system in the photon energy range of 0.015–15 MeV

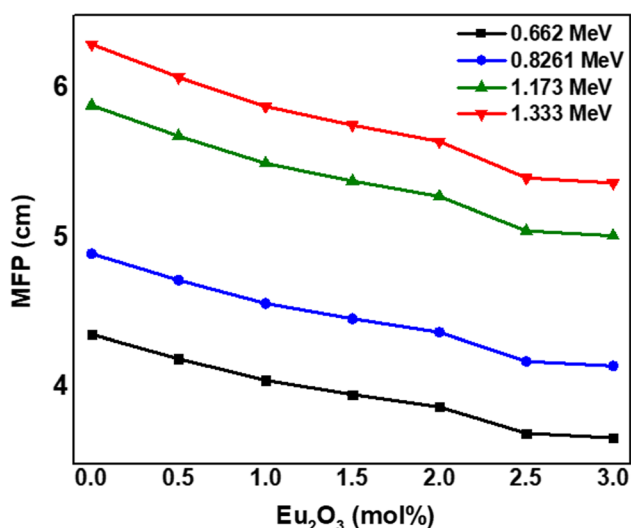


Fig. 8 Graph showing the variation of MFP with Eu_2O_3 mol% at different photon energies

The trend followed by MFP values with radiation energy is the same as HVL. Figure 8 emphasizes the graph of MFP values as a function of Eu_2O_3 concentration at various energies. As the Eu_2O_3 content increased, the MFP values decreased in each case, pointing out the importance of adding the Eu_2O_3 molecules to the glasses. The lowest set of MFP values generated at 0.662 MeV energy proposed that the present glasses attenuate low-energy photons better than the high-energy photons. And since the density value of 3.599 g cm^{-3} produced the lowest MFP values at all the energies, the corresponding Eu7 glass can perform as a better shielding agent in comparison with others. Such dependency of MFP values with Eu^{3+} ion concentration was also observed in previously reported glass systems [6, 7, 53], where glasses containing the highest Eu_2O_3 mol% generated the least MFP.

4. Conclusions

In this research article, the physical, structural, optical, thermal, and radiation shielding properties of the experimental grade finely polished 30 ZnF_2 -20 TeO_2 -(50- x) B_2O_3 - x Eu_2O_3 glasses were studied with $x = 0, 0.5, 1.0, 1.5, 2.0, 2.5, 3.0$ mol% composition. The study focussed on the overall characteristics of the glasses to claim their candidature in generating WLEDs excited through UV or blue LED chips and also to promote its high-temperature resistance for radiation shielding environment (as attenuators against harmful radiation—especially resisting ionizing radiations from harming electronic devices in spacecraft). The physical properties disclosed the possible formation of NBOs in the glass sites through molar

volume, oxygen packing density, and no. of bonds/vol. that were obtained from density and refractive index values. The irregularity in the arrangements of the constituent particles in the glass samples was analysed through the XRD pattern. The outcome of EDS indicated the sample purity and presence of all the expected elements in the same. The zinc fluoro-telluroborate glasses showed good Eu^{3+} solubility up to 3.0 mol%. The absorption intensities of all the bands gradually increased with an increase in the concentration of Eu^{3+} ions in the glass matrix. These samples revealed low ' ΔE ' values, and the ' E_g ' of the samples were studied to be within the range of (2.87–2.67) eV, ensuing a decreasing trend. All the experimented glasses showed $\Delta T \sim (144\text{--}156)^\circ\text{C}$ and $H_f \sim (2.33\text{--}4.0)$, demonstrating its competitive thermal stabilities. The Eu7 glass showcased itself as a better shielding agent than the other glass samples (Eu1–Eu6). Comprehensively, the finest candidature of Eu^{3+} -doped zinc fluoro-telluroborate glasses was examined for optics, photonics, radiation shielding, and also for high-temperature applications.

Funding Open access funding provided by Manipal Academy of Higher Education, Manipal.

Open Access This article is licensed under a Creative Commons Attribution 4.0 International License, which permits use, sharing, adaptation, distribution and reproduction in any medium or format, as long as you give appropriate credit to the original author(s) and the source, provide a link to the Creative Commons licence, and indicate if changes were made. The images or other third party material in this article are included in the article's Creative Commons licence, unless indicated otherwise in a credit line to the material. If material is not included in the article's Creative Commons licence and your intended use is not permitted by statutory regulation or exceeds the permitted use, you will need to obtain permission directly from the copyright holder. To view a copy of this licence, visit <http://creativecommons.org/licenses/by/4.0/>.

References

1. P Suthanthirakumar, C Basavapoornima and K Marimuthu *J. Lumin* **187** 392 (2017)
2. P Suthanthirakumar and K Marimuthu *J. Mol. Struct.* **1125** 443 (2016)
3. G Umamaheswar et al. *J. Lumin.* **207** 201 (2019)
4. K Mariselvam, R A Kumar and V R Rao *Opt. Laser Technol* **118** 37 (2019)
5. Y C Ratnakaram, A Balakrishna, D Rajesh and M Seshadri *J. Mol. Struct.* **1028** 141 (2012)
6. G Jagannath et al. *Optik(Stuttg)* **232** 166563 (2021)
7. H A Saudi, W M Abd-Allah and K S Shaaban *J. Mater. Sci. Mater. Electron.* **31** 6963 (2020)
8. A E Ersundu, M Büyükyıldız, M Ç Ersundu, E Şakar and M Kurudirek *Prog. Nucl. Energy* **104** 280 (2018)
9. D I Tishkevich et al. *Ser. Mater. Sci. Eng.* **848** 012089 (2020)
10. D I Tishkevich et al. *Energy Mater.* **1** 1695 (2018)

11. J P Spratt, G L Schnable and J D Standeven *IEEE J. Solid-State Circuits* **5** 14 (1970)
12. D I Tishkevich et al. *J. Alloys Compd.* **735** 1943 (2018)
13. D I Tishkevich et al. *Nanomaterials* **12** 1 (2022)
14. M Dong et al. *J. Clean. Prod.* **355** 131817 (2022)
15. M Dong et al. *Nucl. Energy* **146** 104155 (2022)
16. G Anjaiah, S N Rasool and P Kistaiah *J. Lumin.* **159** 110 (2015)
17. T O Sales, R J Amjad, C Jacinto and M R Dousti *J. Lumin.* **205** 282 (2019)
18. L Changmin, Y Dianlai, Z Yingying, W Zhiqiang and L Hai *J. Rare Earths* **25** 143 (2007)
19. D Y Aydın, M Gürü, D Ipek and D Özyürek *Arab. J. Sci. and Eng.* **42** 4409 (2017)
20. A Ladaci PhD thesis (University of Lyon, France) (2019)
21. P Suthanthirakumar, S Arunkumar and K Marimuthu *J. Alloys and Compd* **760** 42 (2018)
22. Q Dai, C E Duty and M Z Hu *Small* **6** 1577 (2010)
23. N S Prabhu, V Hegde, M I Sayyed, E Şakar and S D Kamath *Infrared Phys. Technol.* **98** 7 (2019)
24. Y H Elbasha, M M Rashad and D A Rayan *Silicon* **10** 1 115 (2018)
25. F A Moustafa, M Abdel-Baki, A M Fayad and F El-Diasty *Am. J. Mater. Sci.* **4** 119 (2014)
26. M Kuwik, J Pisarska and W A Pisarski *Materials* **13** 4746 (2020)
27. C Wang, J Jiang, J Wang, S Xin, Y Shi and G Zhu *J. Lumin.* **215** 116606 (2019)
28. V R Kumar, G Giridhar and N Veeraiah *Luminescence* **32** 71 (2017)
29. T Wang, W Bian, D Zhou, J Qiu, X Yu and X Xu *Mater. Res. Bull.* **74** 151 (2016)
30. B Fan, J Liu, W Zhou and L Han *J. Lumin.* **215** 116687 (2019)
31. M Bouhadja, N Jakse and A Pasturel *J. Chem. Phys.* **140** 234507 (2014)
32. F A Abdel-Wahab, A M Fayad, M Abdel-Baki and H AbdelMaksoud *J. Non. Cryst. Solids* **500** 84 (2018)
33. K Mariselvam, R A Kumar and P Manasa *Infrared Phys. Technol.* **91** 18 (2018)
34. M A Algrade, M Sultan, O M Samir and A E B Alwany *Appl. Phys. A Mater. Sci.* **123** 524 (2017)
35. V Dimitrov and T Komatsu *J. Univ. Chem. Technol. Metall.* **45** 219 (2010)
36. V Dimitrov and T Komatsu *J. Chem. Technol. Metall.* **48** 549 (2013)
37. V Dimitrov and T Komatsu *J. Non. Cryst. Solids* **249** 160 (1999)
38. V Dimitrov and T Komatsu *J. Non. Cryst. Solids* **356** 258 (2010)
39. V Dimitrov and T Komatsu *J. Solid State Chem.* **196** 574 (2012)
40. M K Halimah, M F Faznny, M N Azlan and H A A Sidek *Results Phys.* **7** 581 (2017)
41. D D Ramteke, K Annapurna, V K Deshpande and R S Gedam *J. Rare Earths* **32** 1148 (2014)
42. A Dwivedi, C Joshi and S B Rai *Opt. Mater. (Amst)* **45** 202 (2015)
43. V R Prasad, M Seshadri, S Babu and Y C Ratnakaram *J. Biol. Chem. Lumin.* **32** 443 (2016)
44. R J Amjad, W Santos, C Jacinto and M R Dousti *J. Lumin.* **192** 827 (2017)
45. V Venkatramu, P Babu and C K Jayasankar *Spectrochim. Acta A: Mol. Biomol. Spectrosc.* **63** 276 (2006)
46. K Mariselvam, R A Kumar and M Jagadeesh *Opt. Mater. (Amst)* **84** 427 (2018)
47. K Mariselvam, R A Kumar and S Karthik *Chem. Phys.* **525** 110379 (2019)
48. M Mirzayi and M H Hekmatshoar *Ionics (Kiel)*. **15** 121 (2009)
49. R Pagoti, S Panda, V Patchapureddy, R K Padhi, B H SubramanianJena and B S Panigrahi *Luminescence* **36** 1706 (2021)
50. D Manzani, J B S Junior, A S Reyna, M L S Neto, J E Q Bautista, S J L Ribeiro and C B de Araújo *Dalt. Trans.* **48** 6261 (2019)
51. A Dehelean, S Rada, I Kacso and E Culea *J. Phys. Chem. Solids* **74** 1235 (2013)
52. E Şakar, Ö F Özpolat, B Alım, M I Sayyed and M Kurudirek *Radiat. Phys. Chem.* **166** 108496 (2020)
53. P E Teresa, K A Naseer, T Piotrowski, K Marimuthu, D A Aloraini, A H Almuqrin and M I Sayyed *Optik(Stuttg)* **247** 168005 (2021)
54. M Kurudirek *J Alloys Compd.* **727** 1227 (2017)
55. M I Sayyed, G Lakshminarayana, I V Kityk and M A Mahdi *Radiat. Phys. Chem.* **139** 33 (2017)
56. A N D'Souza, N S Prabhu, K Sharmila and M I Sayyed *J Non.Cryst. Solids* **542** 120136 (2020)
57. M G Dong, M I Sayyed, G Lakshminarayanac, M Celikbilek Ersundu, A E Ersundu, P Nayare and A Mahdi *J. Non. Cryst. Solids* **468** 12 (2017)

Publisher's Note Springer Nature remains neutral with regard to jurisdictional claims in published maps and institutional affiliations.